Structural−Magnetic Properties Relationship in a New Commensurate Material: $Sr_9Mn_5Co_2O_{21}$

K. Boulahya,† M. Parras,† J. M. González-Calbet,*,† and J. L. Martínez‡

Departamento de Química Inorgánica, Facultad de Químicas, Universidad Complutense, E-28040-Madrid, Spain, and Instituto de Ciencia de Materiales, CSIC, Cantoblanco, E-28049-Madrid, Spain

Received May 12, 2004. Revised Manuscript Received September 9, 2004

Polycrystalline $Sr_9Mn_5Co_2O_{21}$ has been synthesized and characterized by X-ray and electron diffraction, high-resolution electron microscopy, and magnetic measurements. This oxide constitutes the $\alpha = 2\ \beta = 1$ term of the homologous series $(A_3B_2O_6)_\alpha(A_3B_3O_9)_\beta$. Isolated rows of polyhedra sharing faces along the *c*-axis are made up of units of two and three face-sharing octahedra (occupied by Mn) linked by one trigonal prism (occupied by Co) in an ordered way. The chains are separated by columns of Sr atoms. This material behaves as a magnetically disordered system. The magnetic properties suggest antiferromagnetic correlations along the chains, but no long-range magnetic order is achieved.

Introduction

During the past decade, there has been much interest in the structural and magnetic characterization of one-dimensional (1D) oxides structurally related to the hexagonal perovskite 2H-$BaNiO_3$[1] and the K_4CdCl_6[2] structural types. Both structures can be regarded as a hexagonal array of infinite 1D chains of face-sharing polyhedra running parallel to the *c*-axis. In the 2H-type, the polyhedra chains are formed by $[NiO_6]$ octahedra; in Sr_4PtO_6,[3] isotypic to K_4CdCl_6, the chains are formed by the sequence of one $[PtO_6]$ octahedron (Oh) and one $[SrO_6]$[4] trigonal prism (TP). These chains are separated by columns of alkaline-earth atoms.

The ability of both structures to intergrow in an ordered way has played a paramount role on the stabilization of new one-dimensional oxides with different octahedra/trigonal prism ratio. All of them can be considered as members of the $(A_3A'BO_6)_\alpha(A_3B_3O_9)_\beta$[5,6] homologous series in which B stands for octahedrally coordinated cations and A′ refers to cations in TP environment. Structural variety and compositional flexibility are the most remarkable characteristics of this family. At present, at least fifteen structural types[7] have been stabilized with a large variety of metal cations occupying both oxygen environments, the Oh and the TP sites. Among them, various 1D-compounds related to 2H-$BaMnO_3$, that is, where Mn cations are located in the octahedral sites, can be selected. In all these phases containing manganese, a metal of different chemical nature occupies the TP sites. Thus, $Ca_3MnA'O_6$ (A′ = Co, Cu, Ni, Zn)[8−10] compounds constitute the $\alpha = 3\ \beta = 0$ member of the series; $Sr_4Mn_2A'O_9$ (A′ = Mg, Zn, Cu, Ni, Co)[11−15] corresponds to the $\alpha = 3\ \beta = 1$ member; the $\alpha = 3\ \beta = 2$ member is stabilized with the $A_5Mn_3A'O_{12}$ chemical composition,[16] where A = Sr, Ba and A′ = Zn, Ni; and, finally, $Ba_6Mn_4A'O_{15}$ (A′ = Cu, Zn)[17] constitutes the $\alpha = 3\ \beta = 3$ member and $Ba_7Mn_5PdO_{18}$[18] the $\alpha = 3\ \beta = 4$.

Their magnetic properties are usually complex and depend on both the A′ chemical nature and the Oh/TP sequence along the chains. For instance, Ca_3MnCoO_6[8], formed by one octahedron $[MnO_6]$ sharing faces with one $[CoO_6]$ trigonal prism, shows long magnetic ordering of an antiferromagnetic type.[19] Maintaining the same transition metals, Co and Mn, we have recently reported the structural study and magnetic characterization of the $\alpha = 3\ \beta = 1$ member stabilized with a $Sr_4Mn_2CoO_9$

* Corresponding author. E-mail: jgcalbet@quim.ucm.es. Tel: (34) 91 394 43 42/58. Fax: (34) 91 394 43 52.
† Universidad Complutense.
‡ Instituto de Ciencia de Materiales, CSIC.

(1) Lander, J. J. *Acta Crystallogr.* **1951**, *4*, 148.
(2) Bergerhoff, G.; Schmitz-Dumont, O. *Z. Anorg. Allg. Chem.* **1956**, *10*, 284.
(3) Randall, J. L.; Katz, L. *Acta Crystallogr.* **1959** *12*, 519.
(4) Darriet, J.; Subramanian, M. A. *J. Mater. Chem.* **1995**, *5*, 543.
(5) Boulahya, K.; Parras, M.; González-Calbet, J. M. *Chem. Mater.* **2000**, *12*, 25.
(6) Perez-Mato, J. M.; Zakhour, M.; F. Weill, F.; Darriet, J. *J. Mater. Chem.* **1999**, *9*, 2795.
(7) Stitzer, K. E.; Darriet, J.; Zur Loye, H. C. *Curr. Opin. Solid State Mater. Sci.* **2001**, *5*, 535.
(8) Zubkov, V. G.; Bazuev, G. V.; Tyutyunnik, A. P.; Berger, I. F. *J. Solid State Chem.* **2001**, *160*, 293.
(9) Kawasaki, S.; Takano, M.; Inami, J. *J. Solid State Chem.* **1999**, *145* 132.
(10) Bazuev, G. V.; Zubkov, V. G.; Berger, I. F.; Arbuzova, T. I. *Solid State Sci.* **1999**, *1* 365.
(11) Bazuev, G. V.; Zaitseva, N. A.; Krasil'nikov, V. N.; Kellerman, D. G. *Russ. J. Inorg. Chem.* **2003**, *48* (2), 170.
(12) Hernando, M.; Boulahya, K.; Parras, M.; González-Calbet, J. M. *Eur. J. Inorg. Chem.* **2002**, 3190.
(13) El Abed, A.; Gaudin, E.; Darriet, J. *Acta Crystallogr.* **2002**, *C58*, i138.
(14) El Abed, A.; Gaudin, E.; Lemaux, S.; Darriet, J. *Solid State Sci.* **2001**, *3*, 887.
(15) Boulahya, K.; Parras, M.; González-Calbet, J. M.; Martínez, J. L. *Chem. Mater.* **2003**, *15*, 3537.
(16) Hernando, M.; Boulahya, K.; Parras, M.; González-Calbet, J. M.; Amador, U. *Eur. J. Inorg. Chem.* **2003**, 2419.
(17) Cussen, E. J.; Vente, J. F.; Battle, P. D. *J. Am. Chem. Soc.* **1999**, *121*, 3958.
(18) Battle, P. D.; Burley, J. C.; Cussen, E. J.; Darriet, J.; Weill, F. *J. Mater. Chem.* **1999**, *9*, 479.
(19) Rayaprol, S.; Sengupta, K.; Sampathkumaran, E. V. *Solid State Commun.* **2003**, *128*, 79.

10.1021/cm0492538 CCC: $27.50
Published on Web 11/13/2004

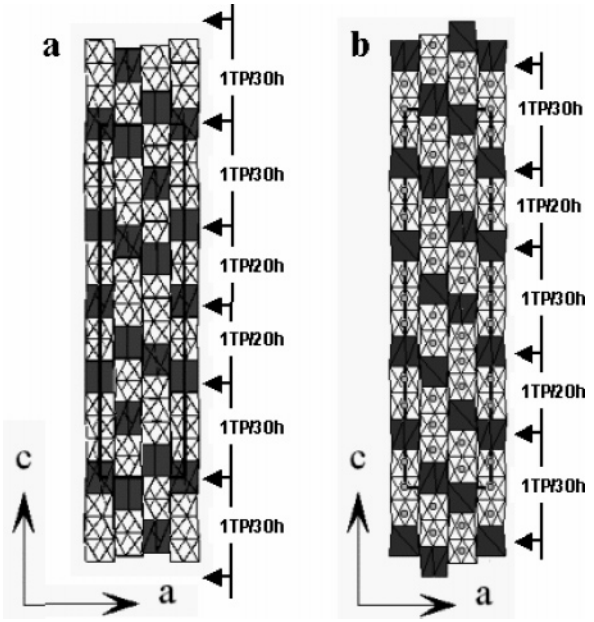

Figure 1. Structural models along *b* axis of (a) $Ba_9Ir_5Cu_2O_{21}$ and (b) $Sr_9Mn_5Ni_2O_{21}$.

chemical composition.[15] This phase is formed by two face-sharing octahedra alternating to one trigonal prism running parallel to the *c*-axis. The magnetic properties seem to indicate strong antiferromagnetic correlations along the chains, but no three-dimensional (3D) magnetic long-range order is observed. This study evidences a complex magnetic nature corresponding to a partially ordered system similar to a magnetic spin glass.

The structural variety of these 1D-phases is nicely reflected in the A-(Co/Mn)-O system. Actually, besides the above phases, the stabilization of two new incommensurate $Sr_{1.2666}(Mn_{0.744}Co_{0.266})O_3$ and $Sr_{1.280}(Mn_{0.728}Co_{0.280})O_3$ materials has been recently reported.[17] These structures are closely related to the idealized compositions $Sr_{14}Mn_8Co_3O_{33}$, $\alpha = 9$ $\beta = 5$, and $Sr_9Mn_5Co_2O_{21}$, $\alpha = 2$ $\beta = 1$, respectively. The first one is isostructural to $Sr_{14}Co_{11}O_{33}$[5,20] and corresponds to an ordered intergrowth of two structural blocks corresponding to the $\alpha = 3$ $\beta = 2$ member, -1TP-3Oh- polyhedra sequence, and one block of the $\alpha = 3$ $\beta = 1$ member, -1TP-2Oh-. On the other hand, for the idealized composition $Sr_9Mn_5Co_2O_{21}$, the proposed structure is that corresponding to $Ba_9Ir_5Cu_2O_{21}$.[21] In this rhombohedral structure, two structural blocks of the $\alpha = 3$ $\beta = 2$ member, constituted by 3Oh-1TP, alternate with two blocks of the $\alpha = 3$ $\beta = 1$ one, -2Oh-1TP-, along the *c*-axis (Figure 1a). It is worth mentioning that for $Sr_9Mn_5Ni_2O_{21}$[16] the polyhedra intergrowth corresponds to the ordered alternance of only one structural block of $\alpha = 3$ $\beta = 2$ with one block of the $\alpha = 3$ $\beta = 1$ (Figure 1a).

It is well-known that the structural features of these 1D-oxides are extremely sensitive to the preparation conditions. Under the synthesis conditions described in the Experimental Section, we have successfully stabilized the commensurate $Sr_9Mn_5Co_2O_{21}$ phase, $\alpha = 2$ $\beta = 1$ member of the homologous series $(A_3A'BO_6)_\alpha$-$(A_3B_3O_9)_\beta$. We report in this paper the crystal structure and physical properties of this new commensurate phase.

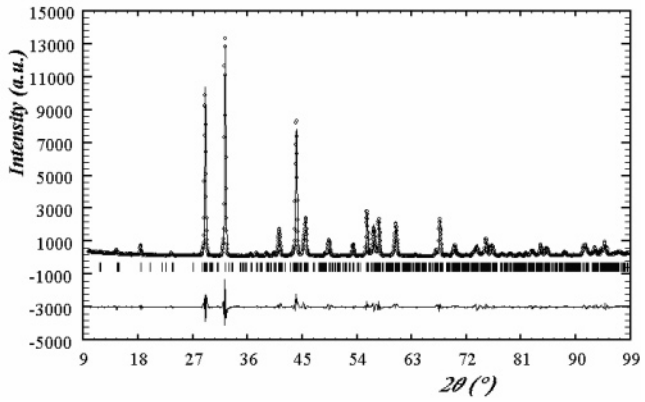

Figure 2. Experimental, calculated, and difference X-ray diffraction pattern for $Sr_9Mn_5Co_2O_{21}$.

Experimental Section

Polycrystalline $Sr_9Mn_5Co_2O_{21}$ was synthesized by heating stoichiometric amounts of $BaCO_3$ (Aldrich 99.98%), Co_3O_4 (Aldrich 99+%), and MnO_2 (Aldrich 99+%) in air at 1200 °C for 7 days and then quenched to room temperature.

Powder X-ray diffraction (XRD) patterns were collected with Cu Kα radiation at room temperature on a PHILIPS X'PERT diffractometer equipped with a graphite monochromator. The diffraction data were analyzed by the Rietveld method[22] using the Fullprof program.[23]

The sample was characterized by SAED and HREM in a JEOL 3000 FEG electron microscope fitted with a double tilting goniometer stage (±22°, ±22°). Local composition was analyzed with an INCA analyzer system attached to the above microscope. Simulated HREM images were calculated by the multislice method using the MacTempas software package.

Magnetic properties were measured in a SQUID magnetometer, in a temperature range from 2 to 300 K, and magnetic fields up to 5 T. The ac magnetic susceptibility was performed either at the SQUID magnetometer or Physical Properties Measurements System (PPMS, QD-San Diego) depending on the excitation frequency, in a range from 0.1 Hz to 10 kHz and a temperature range from 2 to 300 K. The specific heat was measured by the heat pulse relaxation method in a commercial cryostat (PPMS, QD-San Diego) at different external magnetic fields (up to 9 T) with a temperature range from 2 to 200 K. A ceramic pellet of the sample (approximately 7 mg) was attached to a sapphire platform by a small amount of Apiezon N grease (as thermal contact). The signal addenda heat capacity was measured in a separate run and subtracted from the experimental sample data.

Results and Discussion

Structural Characterization. The cationic composition, as analyzed by energy-dispersive X-ray analysis, is in agreement with the nominal composition, $Sr_9Mn_5Co_2O_{21}$. The corresponding X-ray powder diffraction pattern (Figure 2) can be fully indexed on the basis of a 3D rhombohedral unit cell with lattice parameters a = 9.5846 (7) Å, c = 35.9612 (18) Å, with no extra reflections being detected.

Two different 1D-structures, both presenting rhombohedral symmetry, have been previously described for the $A_9B_5A'_2O_{21}$ stoichiometry. In both, the $[A'O_6]$ trigo-

(20) Jordan, N. A.; Battle, P. D.; van Smalen, S.; Wunschel, M. *Chem. Mater.* **2003**, *15*, 4262.
(21) Blake, G. R.; Sloan, J.; Vente, J. F.; Battle, P. D. *Chem. Mater.* **1998**, *10*, 3536.
(22) Rietveld, H. V. *J. Appl. Crystallogr.* **1969**, *2*, 65.
(23) Rodríguez-Carvajal, J. *Physica* **1993**, *B192*, 55.

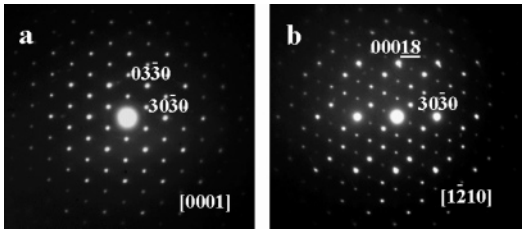

Figure 3. SAED pattern of $Sr_9Mn_5Co_2O_{21}$ (a) along [0001] and (b) along $[1\bar{2}10]$.

nal prisms in the polyhedra chains are separated from each other by dimers (TP-Oh-Oh-TP) and trimers (TP-Oh-Oh-Oh-TP) of $[BO_6]$ face-sharing octahedra. The first one corresponds to the $Ba_9Ir_5Cu_2O_{21}$ structure and it has been described already in the Introduction. As it can be seen in Figure 1a, the polyhedra sequence along the chains is -TP-3Oh-TP-3Oh-TP-2Oh-TP-2Oh-. This compound presents a rhombohedral unit cell ($R32$). The second one corresponds to the structural framework of $Sr_9Ni_7O_{21}$[24] or $Sr_9Mn_5Ni_2O_{21}$,[16] which is formed by the same structural blocks as the previous one, but stacked in a different sequence along the c-axis. Actually, following this direction, one structural unit of (1TP-3Oh) alternates to one of (1TP-2Oh) leading to the -TP-3Oh-TP-2Oh-TP-3Oh-TP-2Oh- sequence (Figure 1b). The unit cell also presents rhombohedral symmetry but different space group ($R\bar{3}c$). To distinguish between the different candidate structures, a microstructural study by means of SAED and HREM, has been performed.

The most relevant reciprocal zone axes, [0001] and $[1\bar{2}10]$, are shown in Figure 3a and b, respectively. All maxima can be indexed on the basis of a rhombohedral lattice with the cell parameters determined from X-ray data, confirming the commensurate nature of our sample. Only the $(-h + k + l) = 3n$; $00l = 6n$ reflections appear. These reflection conditions are compatible with the $R\bar{3}c$ (No. 167) space group. According to that, commensurate $Sr_9Mn_5Co_2O_{21}$ seems to be isostructural to $Sr_9Ni_7O_{21}$ and $Sr_9Mn_5Ni_2O_{21}$. This result is verified by HREM.

The HREM micrograph along the $[1\bar{2}10]$ zone (Figure 4) shows an apparently well ordered material with d spacings 8.3 and 18 Å, corresponding to d_{100} and d_{002}, respectively. Fourier transform was performed on the HREM micrograph, looking for the existence of different domains that could evidence the presence of the $Ba_9Ir_5Cu_2O_{21}$ structure. However, the whole crystal results homogeneous and only the maxima corresponding to the $R\bar{3}c$ symmetry were observed (Figure 4b). Figure 5a corresponds to an enlargement of the experimental image of Figure 4; figure 5b and c show the images calculated from the structural models corresponding to $Sr_9Mn_5Co_2O_{21}$ and $Ba_9Ir_5Cu_2O_{21}$, respectively. Following the c-axis, the contrast variation shown in Figure 5b corresponds to four bright dots alternating with a brighter dot intergrowing in an ordered way with three bright dots alternating with a brighter dot. On the other hand, the calculated image of Figure 5c shows a contrast variation corresponding to two blocks of four bright dots alternating with a brighter one, stacked along the c-axis with two blocks of three bright dots alternating with a

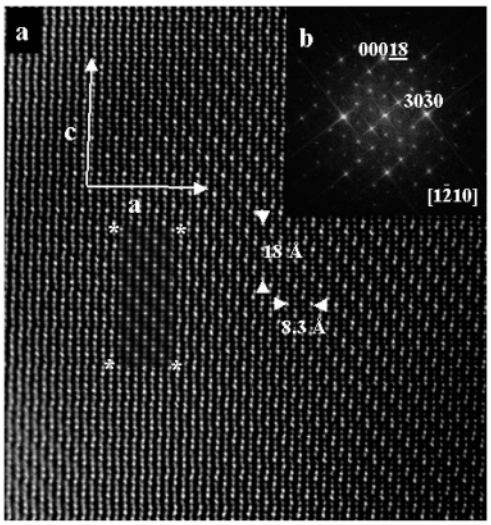

Figure 4. (a) HRTEM image of $Sr_9Mn_5Co_2O_{21}$ along $[1\bar{2}10]$, (b) corresponding FT. Simulated image is shown in the inset.

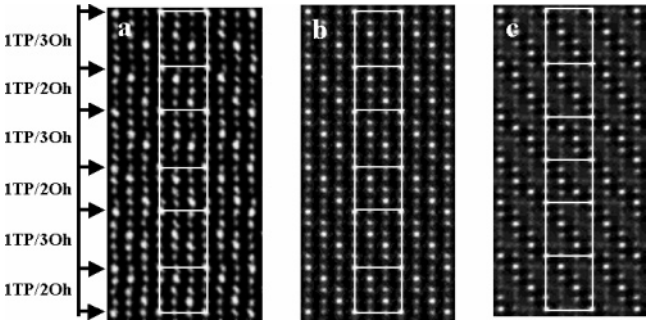

Figure 5. (a) Enlarged experimental image of $Sr_9Mn_5Co_2O_{21}$; (b) simulated image of $Sr_9Mn_5Ni_2O_{21}$, and (c) simulated image of $Ba_9Ir_5Cu_2O_{21}$.

brighter dot. The correspondence between the experimental image (Figure 5a) and the calculated one by using the $Sr_9Mn_5Ni_2O_{21}$ structure (Figure 5b) is clearly shown.

The experimental micrograph is interpreted by considering that, in this $[1\bar{2}10]$ structure projection, Sr atoms overlap with metal cations located in the trigonal prisms, leading to the brightest spots, that, therefore, make evident the positions of the TP polyhedra. According to that, the experimental contrast variation corresponds to the -3Oh-TP-2Oh-TP-3Oh-TP-2Oh- polyhedral sequence. Therefore, from the refined atomic coordinates of $Sr_9Mn_5Co_2O_{21}$ (see next section), an image calculation was performed. The simulated image fits nicely to the experimental one at $\Delta t = 40$ Å and $\Delta f = -700$ Å (shown at the inset of Figure 4a).

Structure Refinement. On the basis of the above results, an X-ray profile refinement of $Sr_9Mn_5Co_2O_{21}$ was performed. The structure was solved in the $R\bar{3}c$ space group taking as starting point the $Sr_9Mn_5Ni_2O_{21}$ crystallographic data;[16] Co and Mn atoms are arranged in the TP and octahedral sites, respectively. Peak shapes were described by pseudo-Voigt functions. Figure 2 shows the graphic results of the fitting of the experimental X-ray diffraction pattern and the difference between observed and calculated data. The refinement was stable and it was possible to refine the positions of oxygen atoms, provided a temperature factor for each type of atoms was used. The final structural parameters

(24) Campá, J.; Gutiérrez-Puebla, E.; Monge, A.; Rasines, I.; Ruiz-Valero, C. *J. Solid State Chem.* **1996**, *126*, 27.

Table 1. Final Structural Parameters of $Sr_9Mn_5Co_2O_{21}$[a]

atom	*x/a*	*y/b*	*z/c*	*B* (Å^2)	occ.
Sr1	0.3224(7)	0.	0.75	1.41 (3)	1
Sr2	0.6472(5)	−0.0004(7)	0.1394(4)	1.41 (3)	1
Co1	0	0	0.3595(6)	1.09(6)	1
Mn1	0	0	0.2157(6)	1.53(4)	1
Mn2	0	0	0.0702(5)	1.53(4)	1
Mn3	0	0	0	1.53(4)	1
O1	0.505(4)	0.315(5)	0.4334(9)	0.42(1)	1
O2	−0.157(6)	0	0.75	0.42(1)	1
O3	0.832(5)	−0.008(6)	0.318(1)	0.42(1)	1
O4	0.503(5)	0.163(5)	0.368(2)	0.42(1)	1

[a] Space group $R\bar{3}c$ (164), a= 9.5891 (7) Å, c= 35.9708 (18) Å, V = 2864.413 (4) Å^3, R_B= 0.052, R_{exp}= 0.069, R_{wp}=0.119, c^2=5.4.

Table 2. Selected Interatomic Distances (Å) in $Sr_9Mn_5Co_2O_{21}$

Sr1−O1: 2.95 (4) × 2	Co1−O1: 2.11 (4) × 3
Sr1−O1: 2.78 (4) × 2	Co1−O3: 2.19 (5) × 3
Sr1−O2: 2.68 (5) × 2	Mn1−O2: 1.91 (5) × 3
Sr1−O3: 2.84 (5) × 2	Mn1−O3: 1.95 (5) × 3
Sr1−O4: 2.43 (4) × 2	Mn2−O1: 1.83 (4) × 3
Sr2−O1: 3.03 (4)	Mn2−O4: 2.00 (5) × 3
Sr2−O1: 2.40 (4)	Mn3−O4: 2.00 (5) × 6
Sr2−O2: 2.61 (2)	Mn1−Co1: 2.74 (3)
Sr2−O3: 2.42 (5)	Mn1−Mn1: 2.47 (3)
Sr2−O3: 2.65 (5)	Mn2−Mn3: 2.49 (1)
Sr2−O3: 2.78 (6)	Mn2−Co1: 2.51 (3)
Sr2−O4: 2.62 (5)	
Sr2−O4: 2.78 (4)	
Sr2−O4: 2.71 (4)	

are collected in Table 1, whereas Table 2 shows some selected interatomic distances. The structure refinement confirms isotypism with $Sr_9Mn_5Ni_2O_{21}$. The essential feature of the structure is the presence of 1D-chains of sharing-faces polyhedra, stacked in the -TP-3Oh-TP-2Oh-TP-3Oh-TP-2Oh- sequence, and folded along the [0001] direction. The chains are separated by columns of Sr atoms. (Figure 1b).

The inter-cation distances Mn−Mn (2.47(6)−2.49(5) Å) and Mn−Co (2.74(3)−2.51(2) Å) within the polynuclear ($Co_2Mn_5O_{21}$) group agree well with those of similar oxides also containing face-sharing polyhedra. For instance, the average Mn−Mn distance in $Sr_4Mn_2NiO_9$ ranges from 2.556 to 2.572 Å[14], while in $Sr_7Mn_4O_{15}$ the corresponding value is 2.53 Å.[25] The Mn−Co distance corresponds to 2.645 Å in Ca_3MnCoO_6[8] and 2.69 Å in $Sr_4Mn_2CoO_6$.[15] The Mn−O distances, 1.85(6) and 2.03(8) Å, are typical for Mn^{4+} octahedra in oxides. For instance, in $Sr_4Mn_3O_{10}$ the Mn−O distances are between 1.77 and 2.10 Å,[26] 1.83−2.05 Å in $Sr_7Mn_4O_{15}$,[25] and 1.85−2.04 Å in $Sr_4Mn_2CoO_9$.[15] Finally, the Sr−O distances (2.40(6)−3.03(5) Å) are close to those observed in other Sr oxides, d(Sr−O) = 2.36−3.02 Å in $Sr_7Mn_4O_{15}$ and 2.33−2.93 in $Sr_4Mn_2CoO_9$.[15]

The ensemble of the XRD, SAED, and HREM results shows that $Sr_9Mn_5Co_2O_{21}$ constitutes a new example of a commensurate 1D oxide. The structural study shows that the polyhedra rows are formed by dimers of octahedra sharing faces linked to trimers through a trigonal prism. The refinement is consistent with Co and Mn occupying the TP and Oh sites, respectively. This regular cationic distribution is reflected in an ordered

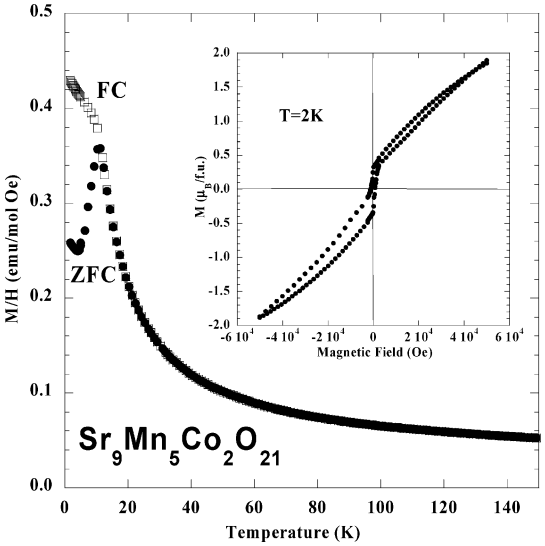

Figure 6. Temperature dependence of the magnetic susceptibility after zero field cooling (ZFC) and field cooling (FC, H = 1 kOe). The inset shows the isothermal magnetization per unit formula for $Sr_9Mn_5Co_2O_{21}$ as a function of the applied magnetic field at 2 K.

microstructure as evidenced by SAED and HREM. The same structural characteristic has been observed in both $Sr_4Mn_2CoO_9$ and Ca_3MnCoO_6.

Physical Properties. $Sr_9Mn_5Co_2O_{21}$ is an insulator with very high resistance even up to 400 K. The magnetic properties are shown in Figure 6. The irreversibility between the zero field cooling and the magnetic field cooling gives rise to a clear peak in the magnetic susceptibility at 10.7 K. The inverse magnetic susceptibility follows a Curie−Weiss law from 50 to 300 K. From this analysis, we extract the value of the paramagnetic moment as 11.7 μ_B/f.u. Assuming a paramagnetic moment for Mn^{4+} of 3.8 μ_B and for Co^{2+} of 4.8 μ_B, and taking into account the total number of magnetic atoms per formula unit, we expect a theoretical value for the paramagnetic moment of 10.9 μ_B/f.u., which is rather close to the experimental one (11.7 μ_B/f.u.). These values could indicate that the formal Mn and Co oxidation states are 4+ and 2+, respectively. According to that, Mn^{4+} is located in octahedral coordination and Co^{2+} is in a trigonal prismatic environment. The obtained value Weiss constant is Θ = −176 K, which indicates that the resulting magnetic interactions are antiferromagnetic-type. The hysteresis loop (presented in the inset Figure 6) shows a remanent magnetization (0.3 μ_B/f.u.) with a hysteretic behavior at higher magnetic fields without reaching saturation (even up to applied magnetic fields of 16 T). For temperatures higher than 11 K, the behavior is linear, similar to that expected for a paramagnetic system. The initial conclusion that we could make from these data is that the system is magnetically disordered without any long-range magnetic ordering.

Similar behavior has been observed in $Sr_4Mn_2CoO_9$.[15] In this compound, dimers of Mn^{4+} in octahedral sites separated by Co^{2+} trigonal prisms constitute the polyhedra rows. The two manganese ions tend to correlate antiferromagnetically. Analogous to that found in $Sr_9Mn_5Co_2O_{21}$, no long range 3D antiferromagnetic order is achieved through the Co ions. However, this long range 3D order is observed in Ca_3MnCoO_6[8] at temper-

(25) Vente, J. F.; Kamenev, K. V.; Sokolov, D. A. *Phys. Rev.* B **2002**, *64*, 214403.
(26) Floros, N.; Hervieu, M.; van Tendeloo, G.; Michel, C.; Maignan, A.; Raveau, B. *Solid State Sci.* **2000**, *2*, 1.

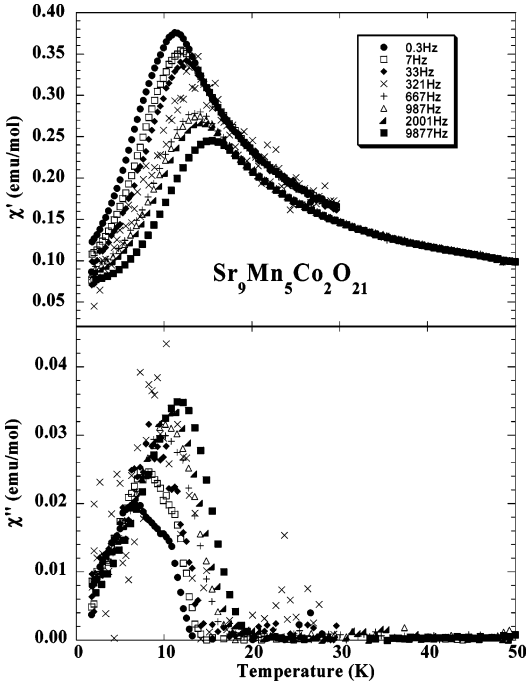

Figure 7. Upper frame: Temperature dependence of the real part of the ac magnetic susceptibility for frequencies in the range from 0.1 Hz to 10 kHz. Lower frame: Imaginary part of the ac magnetic susceptibility for $Sr_9Mn_5Co_2O_{21}$ on the same conditions.

atures close to 13 K. The larger radius of strontium increases the interchain distances probably avoiding the 3D order and giving rise to a disordered magnetic state at low temperatures.

For magnetic systems with no long-range magnetic ordering, the ac magnetic susceptibility is an important tool to study the time response of the magnetic system. In Figure 7 we present the real and imaginary part of the magnetic susceptibility for a wide range of excitation frequencies, which span 6 orders of magnitude (10^{-1} to 10^4 Hz), for an excitation amplitude of 1 Oe. Both signals present a clear maximum at 10.7 K (0.3 Hz) that shifts to 16.1 K at higher frequencies (9.8 kHz). The dispersion of the susceptibility for different frequencies is clear below the peak, and all the data tend to collapse to a single curve for temperatures above the maximum. This suggests that at high temperature the system behaves as a normal paramagnetic system following the frequency of the excitation magnetic field. Below the peak temperature, the different magnetic clusters behave differently as a function of the frequency of the magnetic field.

To unambiguously discard the presence of any long-range magnetic ordering we have measured the specific heat at low temperature under applied magnetic field. To extract the magnetic part of the specific heat (separated from the phononic and electronic contribution), we should measure a similar sample (same structure) with no magnetic ions. In our case, this option is almost impossible, so we opted to use a different approach to obtain the magnetic part of the specific heat. We applied a strong magnetic field (9 T) and we assumed that this field was enough to saturate any magnetic component, so that the entropy variation related to the magnetic ordering should be spread along a very wide temperature range. In this approximation,

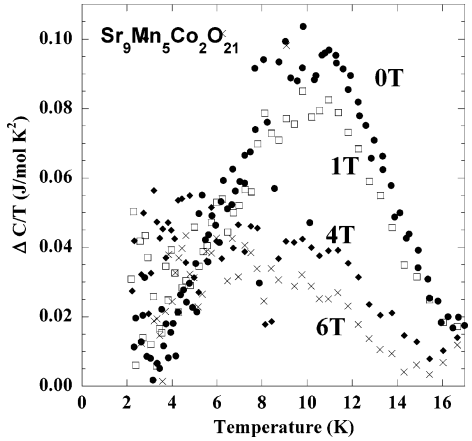

Figure 8. Temperature dependence of the magnetic part of the specific heat at different applied magnetic fields for $Sr_9Mn_5Co_2O_{21}$.

we could use the high field specific heat as the specific heat background for the zero field data and other intermediate magnetic fields. In that way, we measured the specific heat at different magnetic fields down to zero magnetic field. The magnetic and specific heat (after subtracting the specific heat at 9 T) data are presented in Figure 8 for different applied magnetic fields (0, 1, 4, and 6 T). A clear, but weak peak is observed at approximately 10 K (0 T), that shifts to a lower temperature (8 K) at higher magnetic fields (6 T). For zero magnetic field, the integration of the peak gives rise to a magnetic entropy of 0.8 J/mol K. This entropy is only a tiny fraction of the expected entropy for a long-range magnetic ordering for 5 ions Mn^{4+} ($S = {}^3/_2$) and 2 ions Co^{2+} ($S = {}^3/_2$). In that sense, the specific heat data also confirm that $Sr_9Mn_5Co_2O_{21}$ is a magnetically disordered system, similar to a spin glass with strong frequency dependence below the freezing temperature (10.7 K). The magnetic properties in $Sr_9Mn_5Co_2O_{21}$ are analogous to those previously reported for $Sr_4Mn_2CoO_9$. This latter oxide behaves as a partially ordered system, close to a magnetic spin glass. The entropy associated with this partial magnetic order is also smaller than that corresponding to the ordered state but higher than that obtained for $Sr_9Mn_5Co_2O_{21}$ which behaves as a more disordered magnetic system.

The above results allow comparison of the magnetic behavior of the three 1D commensurate oxides up to now reported containing Mn^{4+} and Co^{2+} in octahedral and prismatic oxygen coordination, respectively. The polyhedra chains of Ca_3CoMnO_6 are formed by the sequence of $-(Mn^{4+})_{Oh}-(Co^{2+})_{TP}-(Mn^{4+})_{Oh}-(Co^{2+})_{TP}-$, separated by columns of Ca^{2+}. The small size of this AE metal leads to small interchain distances. As a consequence, a long-range 3D antiferromagnetic order is attained at 13 K.[8] Following the series, the increase of the number of octahedra between prisms gives rise to more complex magnetic systems. This is the case for $Sr_4Mn_2CoO_9$,[15] where the 1D chains are composed by two face-sharing octahedra (with Mn^{4+}) and one trigonal prism (with Co^{2+}); the chains are now separated by strontium with higher ionic radius than calcium. In that case, the long-range magnetic ordering is lost, although a clear peak related to large magnetic clusters (short-range magnetic order that could reach a complete 1D chain, but no long-range magnetic coupling between

chains) is observed at 10 K with a noticeable anomaly at the magnetic part of the specific heat.[12] The present compound ($Sr_9Mn_5Co_2O_{21}$) is also rather complex because the chains are composed by a polyhedra sequence of three face-sharing octahedra (Mn^{4+}), followed by one trigonal prism (Co^{2+}), and finally, two face-sharing octahedra (Mn^{4+}); as in the previous phase, strontium ions separate the polyhedra chains. Therefore, the total magnetic unit is a trimer and a dimer of Mn ions separated by a Co prism. Obviously, the distances and angles inside the dimers and trimers are different, increasing the magnetic disorder. As a consequence, the long-range magnetic order is not present, and the short-range magnetic order is rather small (magnetic clusters of small size), compared to the previous compound ($Sr_4Mn_2CoO_9$). According to that, as observed in Figure 8, the anomaly and the associated entropy on the magnetic part of the specific heat is rather weak for $Sr_9Mn_5Co_2O_{21}$.

Acknowledgment. Financial support through research projects MAT2001-1440 and MAT2002-1329 is acknowledged. K.B. thanks the MCYT (Spain) for financial support under the "Ramón y Cajal" Program.

CM0492538